Astron. Astrophys. 354, 787–801 (2000)

ASTRONOMY AND ASTROPHYSICS

A study of the cool gas in the Large Magellanic Cloud

I. Properties of the cool atomic phase – a third H I absorption survey

M. Marx-Zimmer[1], **U. Herbstmeier**[2], **J.M. Dickey**[3], **F. Zimmer**[1], **L. Staveley-Smith**[4], **and U. Mebold**[1]

[1] Radioastronomisches Institut der Universität Bonn, Auf dem Hügel 71, 53121 Bonn, Germany
[2] Max-Planck-Institut für Astronomie, Königstuhl 17, 69117 Heidelberg, Germany
[3] Department of Astronomy, University of Minnesota, Minneapolis, MN 55455, USA
[4] Australia Telescope National Facility, P.O. Box 76, Epping, NSW 2121, Australia

Received 16 November 1998 / Accepted 20 April 1999

Abstract. The cool atomic interstellar medium of the Large Magellanic Cloud (LMC) seems to be quite different from that in the Milky Way. In a series of three papers we study the properties of the cool atomic hydrogen in the LMC (Paper I), its relation to molecular clouds using SEST-CO-observations (Paper II) and the cooling mechanism of the atomic gas based on ISO-[C II]-investigations (Paper III).

In this paper we present the results of a third 21 cm absorption line survey toward the LMC carried out with the Australia Telescope Compact Array[1] (ATCA). 20 compact continuum sources, which are mainly in the direction of the supergiant shell LMC 4, toward the surroundings of 30 Doradus and toward the eastern steep H I boundary, have been chosen from the 1.4 GHz snapshot continuum survey of Marx et al. We have identified 20 absorption features toward nine of the 20 sources. The properties of the cool H I clouds are investigated and are compared for the different regions of the LMC taking the results of Dickey et al. (survey 2) into account.

We find that the cool H I gas in the LMC is either unusually abundant compared to the cool atomic phase of the Milky Way or the gas is clearly colder ($T_c \approx 30$ K) than that in our Galaxy ($T_c \approx 60$ K). The properties of atomic clouds toward 30 Doradus and LMC 4 suggest a higher cooling rate in these regions compared to other parts of the LMC, probably due to an enhanced pressure near the shock fronts of LMC 4 and 30 Doradus. The detected cool atomic gas toward the eastern steep H I boundary might be the result of a high compression of gas at the leading edge.

Key words: galaxies: Magellanic Clouds – ISM: general – galaxies: ISM – radio lines: galaxies

1. Introduction

In the Large Magellanic Cloud a more intense UV radiation field coupled with a lower heavy-element abundance and a lower dust-to-gas ratio leads to an interstellar medium which is quite different from that in the Galaxy. The properties of molecular clouds are affected as well as those of the atomic gas. Studying the influence on the cool atomic phase is of special significance as cool atomic clouds can become the raw material for star formation and so determine the evolution of the whole galaxy.

The investigation of the cool atomic gas in the Magellanic Clouds started with a 21 cm absorption line survey using the ATCA toward continuum sources in or behind the H I halo around the Magellanic Clouds and toward the Magellanic Stream (Mebold et al. 1991). No H I absorption features were detected, indicating that all of the atomic hydrogen outside the optical boundaries of the Magellanic Clouds is in the warm phase. With lower spin temperature limits as high as 600 K, the diffuse gas in the halo of the Magellanic Clouds and in the Magellanic Stream appears warmer than that in the outer parts of our Galaxy.

In a second H I absorption line survey (Dickey et al. 1994, hereafter survey 2) the search for cool atomic gas has been extended to the inner part of the LMC. A large number of cool H I clouds were detected. Out of a sample of 30 compact sources we have identified 42 absorption features toward 19 sources. The comparison of the ATCA-H I-absorption spectra and Parkes-emission spectra near the sources yield spin temperatures between 4 K and 100 K. The mean temperature of 25 K is much below that found for H I clouds in the Milky Way ($T_c \approx 60$ K, Kalberla et al. 1985). In a more detailed analysis of cloud temperatures near 30 Doradus, Mebold et al. (1997) compared ATCA absorption spectra with high resolution emission data near the sources and also derived low temperatures between 30 K and 40 K for the cool atomic gas. The energy balance of these cool clouds, some of which are located in warm surroundings, is still an open question. The mixture of the warm and cool phases depends critically on the gas pressure and on other physical parameters such as the heavy-element and dust abundance and the strength of the interstellar radiation field (Wolfire et al. 1995). The distribution of the cool H I gas in the LMC is in sharp contrast to the CO survey of Cohen et al. (1988) and the [C II] observations of Mochizuki et al. (1994), which show that only a few of the H I clouds have emission by heavy elements.

Send offprint requests to: M. Marx-Zimmer

[1] The Australia Telescope is funded by the Commonwealth of Australia for operation as a National Facility managed by CSIRO

The unusually high fraction of cool H I near 30 Doradus and the detection of cool gas near LMC 4 and the eastern steep H I boundary raises the question whether cool gas is abundant in these regions due to a high pressure. Such a high pressure is expected near LMC 4, generated by the supernova driven shocks in this supergiant shell. Several H I shells have also recently been detected near 30 Doradus by Düsterberg et al. (in prep.). At the eastern steep H I boundary the pressure might be increased, because of the motion of the LMC through the halo of our Galaxy at rather high velocity (Mathewson & Ford 1984).

In the present third H I absorption survey toward 20 continuum sources in and behind the LMC we therefore studied the cool phase near LMC 4 and the eastern H I boundary in more detail and extended our investigation of cool H I to the vicinity of the Tarantula nebula. The physical properties of the cool H I clouds for these different regions of the LMC are determined and the spatial distribution of the abundance of the cool gas phase with regard to the locations within the LMC is investigated taking into account the results of survey 2. In two following papers we will study the relation between the cool atomic and molecular phases based on SEST-CO-observations (Paper II) and the heating/cooling balance using ISO-[C II]-observations (Paper III).

In Sect. 2 the observing and data reduction procedures are described. The individual absorption spectra are presented in Sect. 3 and are discussed in relation to the local conditions along each line of sight through the LMC. The fraction of cool gas compared to warm, as revealed by the integrals of the absorption and emission spectra, is investigated in Sect. 4.1 and is compared with results from the Milky Way. In Sect. 4.2 the properties of individual clouds are examined and a comparison of cloud parameters for the different regions of the LMC (the 30 Doradus complex, LMC 4, the eastern steep H I boundary) is given.

2. Observation and data reduction

The 21 cm absorption survey has been done toward 20 compact continuum sources, which have been selected from our ATCA snapshot survey at 1.4 GHz (Marx et al. 1997). The sources are mainly in directions near the 30 Doradus complex, the Hα supergiant shell LMC 4, and in the direction of the sharp H I edge at the eastern boundary of the LMC. These regions are illustrated on the Hα image of the LMC in Fig. 1, together with the location of the continuum sources. In Table 1 the positions of the sources are listed, Columns 2–5. The X and Y coordinates (Columns 4 and 5) are offsets in degrees toward the centre of the rectangular grid defined by Isserstedt (1975). The peak flux densities, which are between 21 and 80 mJy, are given in Column 6 (uncorrected for primary beam attenuation). The noise in the optical depth, σ_τ, is shown in Column 7. The locations of the background sources with regard to the prominent structures are given in Column 8. "Others" are lines of sight, which we use as a reference sample, as they are far distant from the 30 Doradus region, LMC 4 and the eastern H I boundary. Source names (Column 9) are taken from our catalogue of compact continuum sources (Marx et al. 1997). Source No. 18 has not been selected from this snapshot survey, but was within the primary beam of one line of sight at the far east during the H I absorption study.

The spectral line observations were made in May 1994 using the single 6 km configuration (6D) of the ATCA. The resulting synthesized beamwidth is $\sim 7''$. A spectrometer configuration with 4 MHz bandwidth divided into 1024 channels was used. This gives a channel separation of 3.9 kHz = 0.825 $\mathrm{km\,s^{-1}}$. The central frequency was 1419 MHz, which translates to a centre velocity of $v_{\rm LSR}$ = 283 $\mathrm{km\,s^{-1}}$. We have integrated two to seven hours on each source, depending on its continuum flux density, with individual scans of $\approx$ 10 min each, spread over various hour angles to give the best uv-coverage. This provides an optical depth sensitivity σ_τ between 0.1 and 0.25. As primary flux and bandpass calibration source we used B1934-638, the secondary (phase and gain) calibrator was B0407-658. The calibration was done using the AT version of the Astronomical Image Processing System (AIPS). To reduce the noise in the spectra we averaged together every two channels using the AIPS task 'AVSPC'. The final spectra have the same velocity resolution of 1.65 $\mathrm{km\,s^{-1}}$ as those of survey 2. The absorption spectra were computed using the task POSSM with vector averaging, shifting to the centre position of each source as computed from the continuum maps. A linear baseline was fitted to the velocity ranges 43–108 $\mathrm{km\,s^{-1}}$ and 439–504 $\mathrm{km\,s^{-1}}$, which are free of emission and absorption from either Galactic or Magellanic H I. Only baselines longer than 3 kλ (796 m) were used, so as to filter out emission features as far as possible. Since POSSM gives the resultant amplitude and phase of the vector averaged complex visibility function it is necessary to correct for the noise vector as described in Thompson et al. (1986, Eq. 9.46–9.52). For this correction the approximations of Dickey et al. (1994) have been used.

By rejecting data from baselines shorter than 3 kλ we are effectively filtering the image of the LMC to pass only the higher spatial frequencies. The equivalent largest angular size to which we are sensitive is $70''$, or 17 pc at a distance of 50 kpc. The background sources are much smaller than this, so the absorption spectra are not effected by the cutoff, except to slightly raise the noise because of the rejected data. However, including shorter baselines would pollute the spectra with "pseudo-absorption" (Radhakrishnan et al. 1972), which is a figment of small scale structure in the emission. We can estimate the level of such pollution from the study of the spatial power spectrum of the HI emission in the SMC by Stanimirovic et al. (1999). Although emission fluctuations are not detected at such long baselines, if we assume that the power law dependence of amplitude vs. baseline length seen for shorter baselines continues to such small angular sizes, then the maximum amplitude expected for the emission fluctuations would be well below 100 mJy. Since these fluctuations occur with random phases all over the primary beam, they integrate down toward a mean of zero. The absence of positive features in the absorption spectra shows that, with our cutoff, confusion by emission fluctuations is not a problem. Typically, the amplitude of the emission fluctuations is proportional to the overall amplitude of the emission (unless

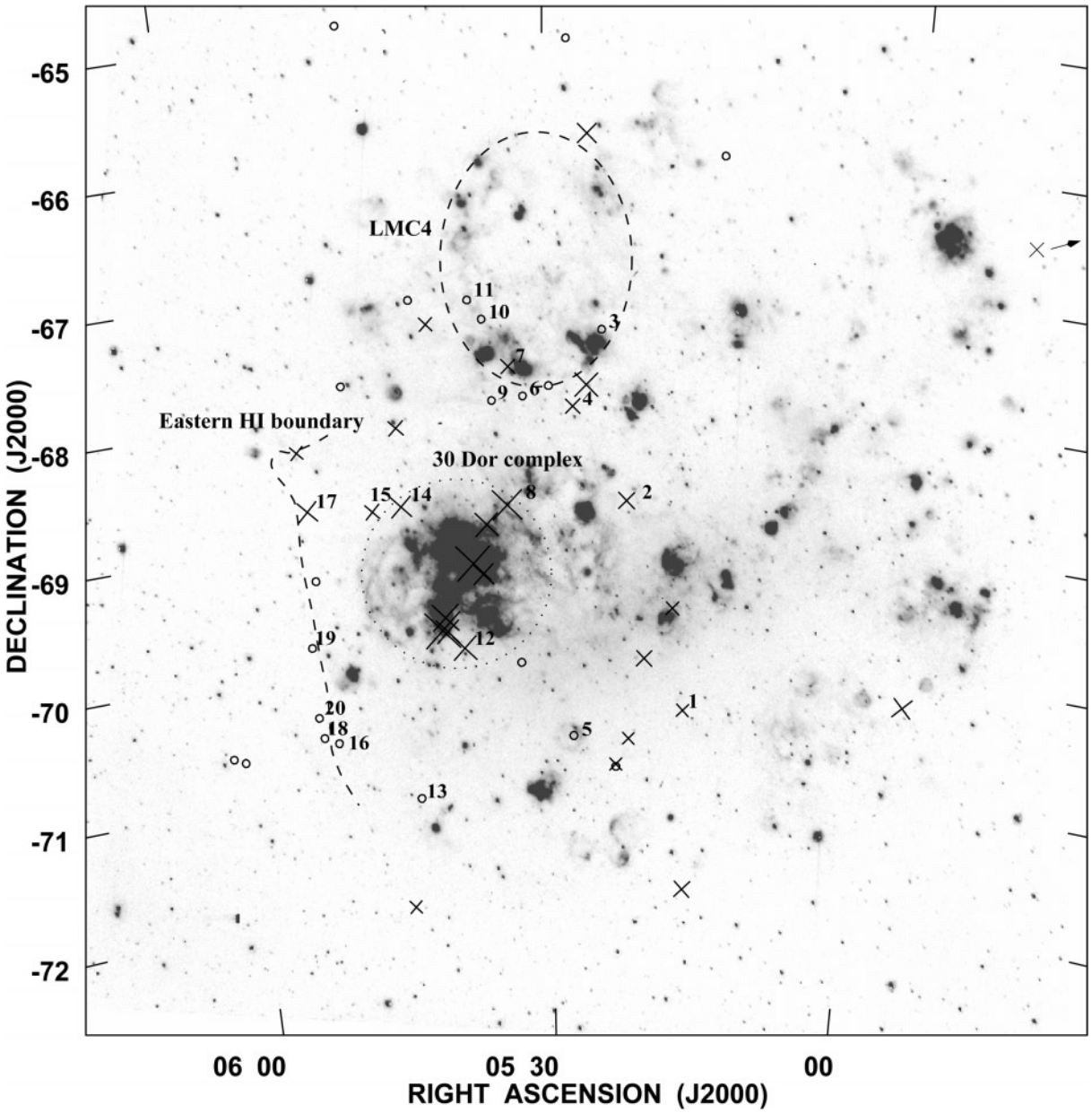

Fig. 1. Locations of the background sources used for H I absorption surveys 2 & 3 are superposed on the Hα image of the LMC from Kennicutt et al. (1995). Numbers at the upper right of the symbols indicate the new data. The positions showing no cool gas above the detection threshold are marked by circles; crosses describe the positions with detected absorption. The size of these symbols is proportional to the absorption integral. The optical boundary of the supergiant shell LMC 4 is sketched with dashed lines. The region, which we call the 30 Doradus complex, is indicated with dotted lines. The eastern H I boundary of the LMC is marked by the 30 % level of the maximum of the total H I column density observed by Luks & Rohlfs (1992, see also Fig. 3).

the optical depth is very high, which never occurs in the Magellanic Clouds except perhaps in 30 Dor itself). Thus regions of low emission brightness are even less subject to confusion in this way than the regions of higher HI line strength.

3. Results

3.1. The spectra

The absorption spectra are presented in Fig. 2a-t together with the 21 cm emission spectra in the direction of the continuum sources. The 21 cm emission data were taken from the survey of Luks & Rohlfs (1992, see also Fig. 3), which has a spatial resolution of $15'$ (=200 pc) and a velocity resolution of $1\,\mathrm{km\,s^{-1}}$. Fourier interpolation has been used to resample the spectra

Table 1. Background sources

Source No.	R.A. (J2000) [h m s]	Dec. (J2000) [° ′ ″]	X	Y	$S_{\rm p}$ [mJy]	σ_τ	Region	Identification
(1)	(2)	(3)	(4)	(5)	(6)	(7)	(8)	(9)
1	05 17 15.9	-70 23 56.8	-0.56	-0.67	80	0.13	Others	MDM 1
2	05 22 58.8	-68 44 27.7	-0.09	1.00	26	0.23	Others	MDM 20
3	05 25 17.3	-67 22 46.6	0.12	2.40	65	0.14	LMC 4	MDM 25
4	05 27 45.9	-67 59 25.7	0.35	1.76	58	0.13	LMC 4	MDM 31
5	05 27 49.1	-70 36 42.9	0.32	-0.87	44	0.15	Others	MDM 32
6	05 32 06.9	-67 54 13.0	0.76	1.84	37	0.18	LMC 4	MDM 44
7	05 33 18.5	-67 39 58.6	0.88	2.07	46	0.16	LMC 4	MDM 55
8	05 33 42.2	-68 46 03.5	0.88	0.97	21	0.16	30 Dor (intrinsic)	MDM 56
9	05 34 48.3	-67 55 58.5	1.01	1.80	28	0.25	LMC 4	MDM 58
10	05 35 26.7	-67 17 03.5	1.10	2.45	54	0.16	LMC 4	MDM 60
11	05 36 36.3	-67 07 35.3	1.22	2.60	68	0.11	LMC 4	MDM 64
12	05 38 04.8	-69 53 36.8	1.21	-0.17	72	0.12	30 Dor	MDM 68
13	05 43 06.8	-71 04 02.8	1.55	-1.36	44	0.20	Others	MDM 88
14	05 43 14.5	-68 44 35.7	1.74	0.94	62	0.10	30 Dor	MDM 89
15	05 45 50.4	-68 45 56.7	1.97	0.92	60	0.12	Others	MDM 95
16	05 50 48.5	-70 34 33.0	2.22	-0.92	32	0.17	Eastern Edge	MDM 109
17	05 51 39.2	-68 43 14.8	2.50	0.91	47	0.18	Eastern Edge	MDM 111
18	05 52 09.7	-70 31 27.3	2.34	-0.88	24	0.20	Eastern Edge	
19	05 52 27.6	-69 48 00.7	2.45	-0.17	73	0.15	Eastern Edge	MDM 113
20	05 52 28.7	-70 21 33.9	2.39	-0.72	49	0.22	Eastern Edge	MDM 114

with channel centres and widths corresponding to the absorption spectra. When comparing the absorption component with the emission we take the two component model of Luks and Rohlfs into account. Their spectra in general show two main components, the principle velocity component (disk- or "D" component) of the LMC emission, which can be fitted well by a differentially rotating disk with a simple rotation curve and an inclination of 33° and a low velocity gas layer, the "L" component, which is mainly found at the east side of the LMC.

The 30 Doradus complex

There are three sources in the vicinity of the Tarantula nebula, a region of intense star formation including 30 Doradus (DEM263, N157), DEM271 (N159) and DEM284 (N160). It is located at the northern part of the giant H I cloud of high column density observed by Luks and Rohlfs (see Fig. 3). An exceptional velocity distribution of cool H I is found at all lines of sight toward the 30 Doradus complex.

Source **MDM 68 (No. 12)** is in the direction of the giant molecular cloud, about 14′.2 from DEM 271 (N159). It shows several deep absorption line components covering a velocity range similar to that of J0539-697 and J0540-697 in N159 (see survey 2).

Source **MDM 56 (Nr. 8)** has a projected distance of 500 pc from 30 Doradus and is lying in the direction of DEM233 (N150). The detection of a small molecular cloud and a compact Hα knot toward MDM 56 indicates a young star forming region, still embedded in a dense cold cloud (Paper II). The absorption spectrum shows one very deep and broad line, which seems to be a blend of several narrower lines. It is offset from the emission ("L" component) by about 7 $\mathrm{km\,s^{-1}}$, indicating a very low spin temperature of the atomic gas of only 10 K (Sect. 4). No absorption is seen at the velocity of the "D" component in direction of this intrinsic source. This might support the result of Blondiau et al. (1997), who find the "L" component to be located in front of the "D" component. Source J0535-689 (survey 2), which is about 200 pc south-west of MDM 56, shows absorption at similar velocities but with smaller equivalent width.

Source **MDM 89 (No. 14)** has a projected distance of 440 pc from 30 Doradus and is about 12′ north of DEM 299 (N165), an ionized gas ring of 80 pc diameter. The spectrum reveals a deep band of absorption, which might be a blend of several narrower lines, covering velocities from about 258 to 276 $\mathrm{km\,s^{-1}}$. The deep absorption components at 258 $\mathrm{km\,s^{-1}}$ and at 264 $\mathrm{km\,s^{-1}}$ have velocities similar to the ionized hydrogen near N165 (Caulet et al. 1982).

Supergiant shell LMC 4

Seven lines of sight of our H I absorption survey (No. 3, No. 4, No. 6, No. 7, No. 9, No. 10 and No. 11) are near to LMC 4, the largest supergiant shell in the LMC. The Hα filaments and H II regions of this complex pattern, located in the northern part of the LMC, form an almost perfect ring with a diameter of 1.4 kpc (1.6°) centered at 05h31m, -66°55′ (1950) (Meaburn 1980). The disk H I of the shell shows a ringlike structure, 1.8 kpc in diameter with a very pronounced central hole (Dopita et al. 1985). The energetics of the whole region strongly suggest that massive stars generate a local overpressure in the interstellar medium, which drives a shock in the intercloud medium,

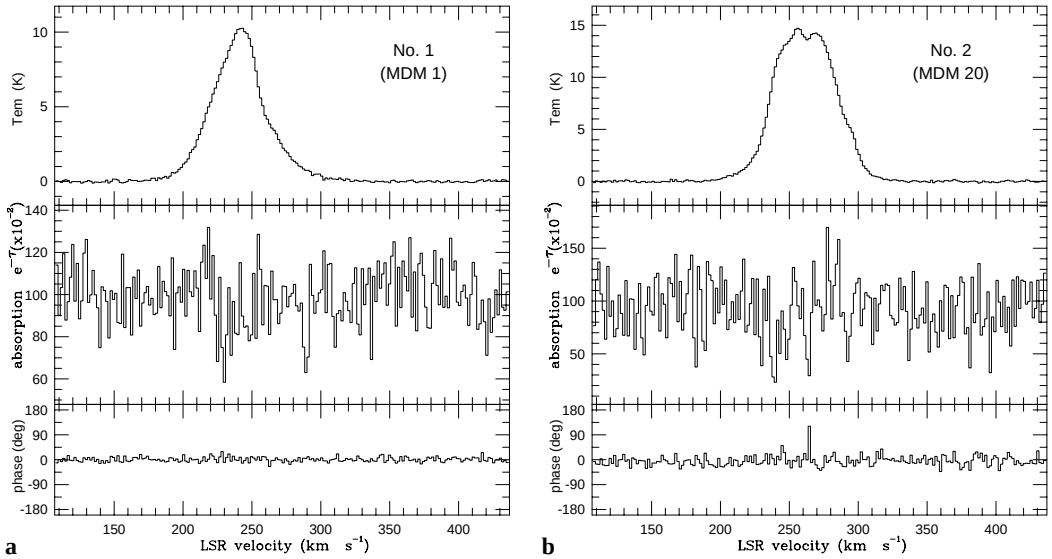

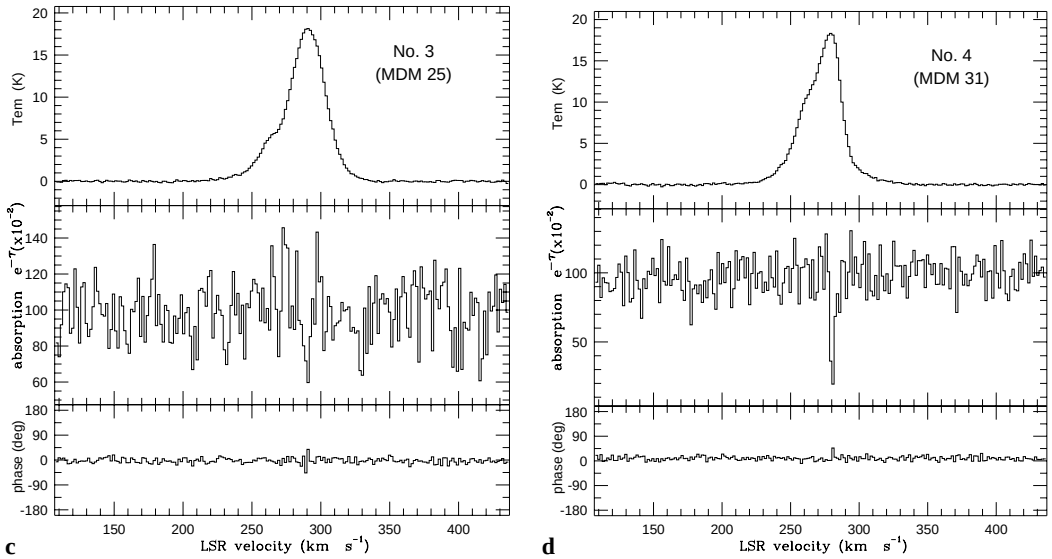

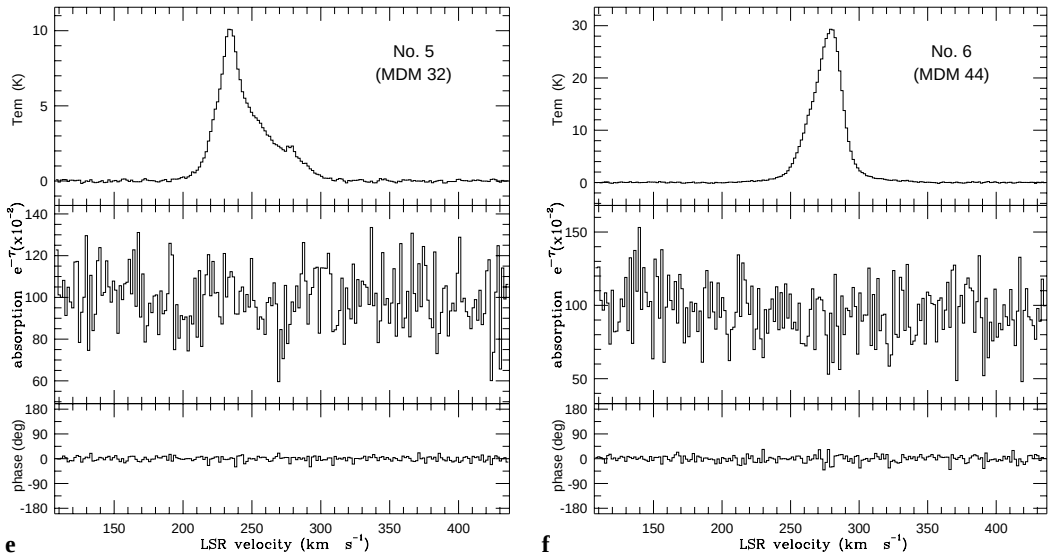

Fig. 2a–t. See page 794

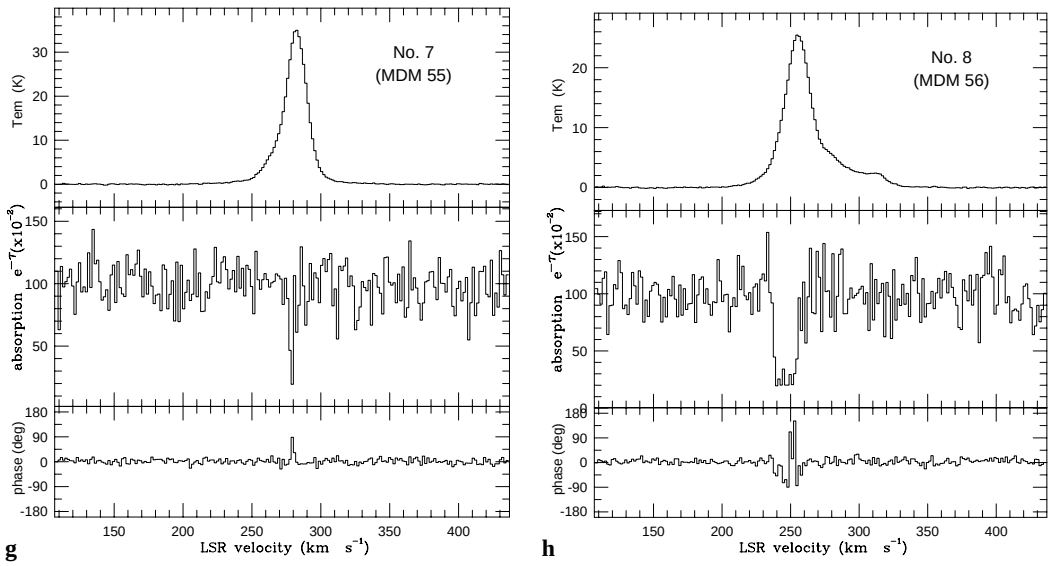

g h

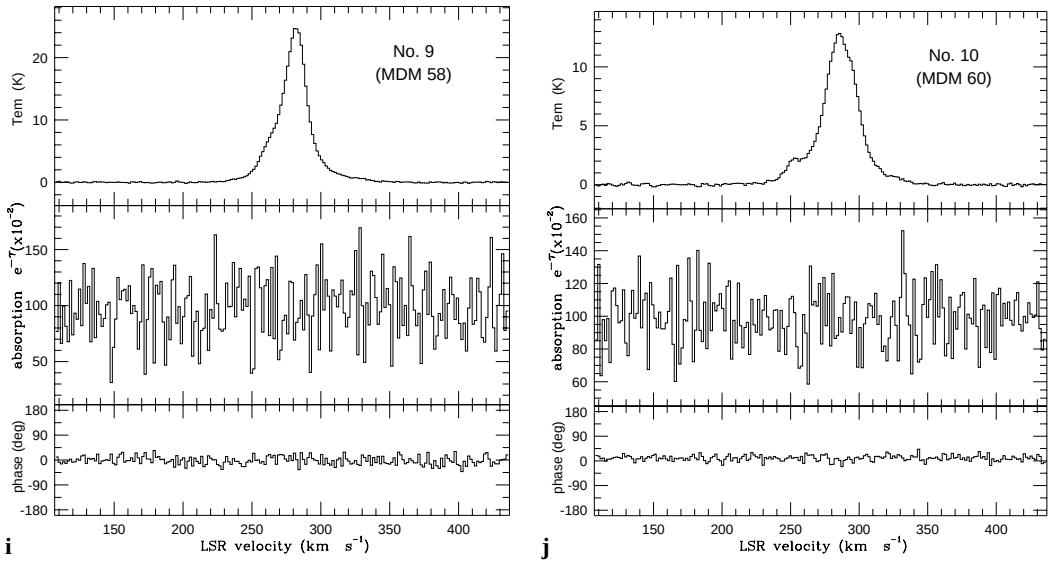

i j

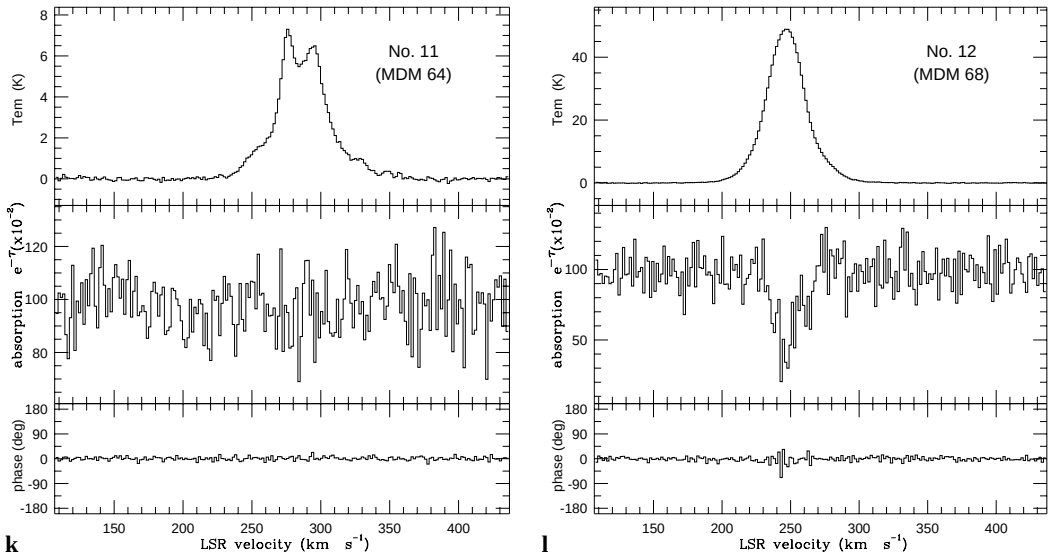

k l

Fig. 2a–t. See page 794

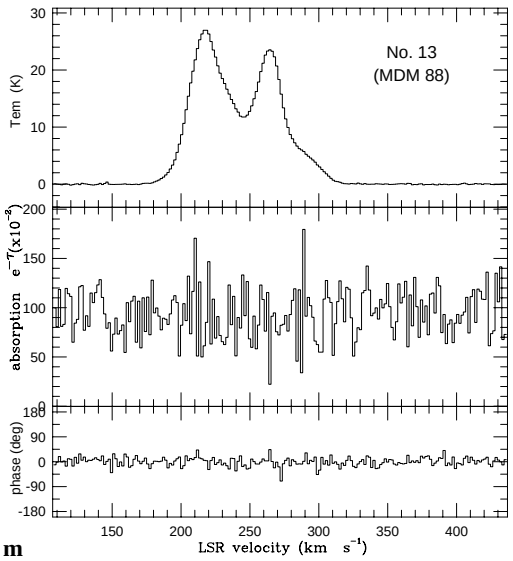

m

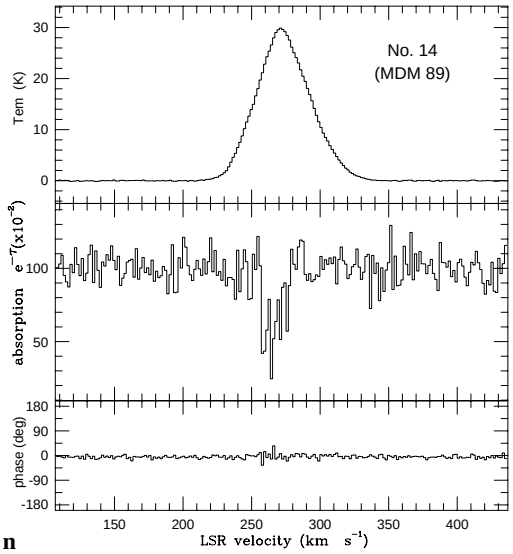

n

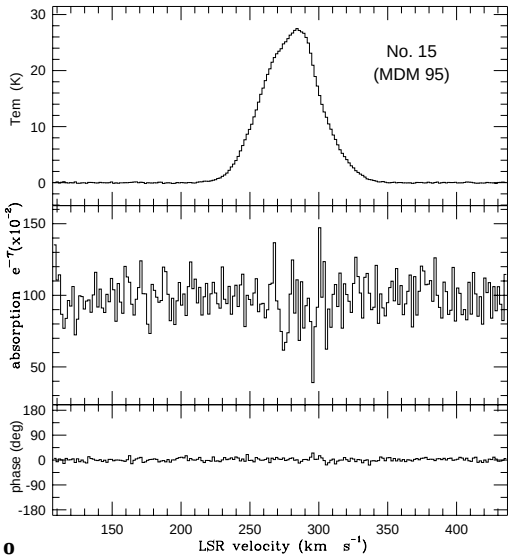

o

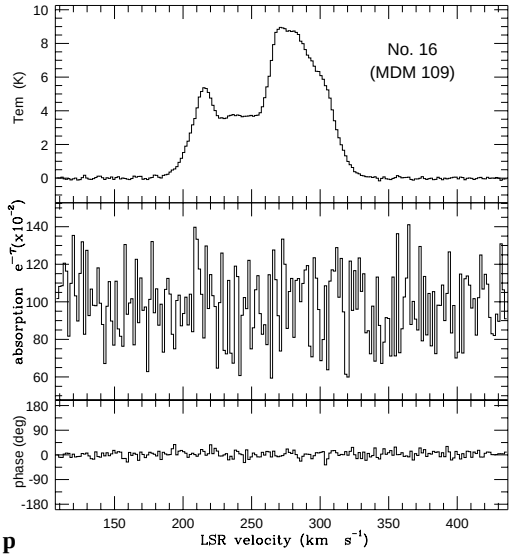

p

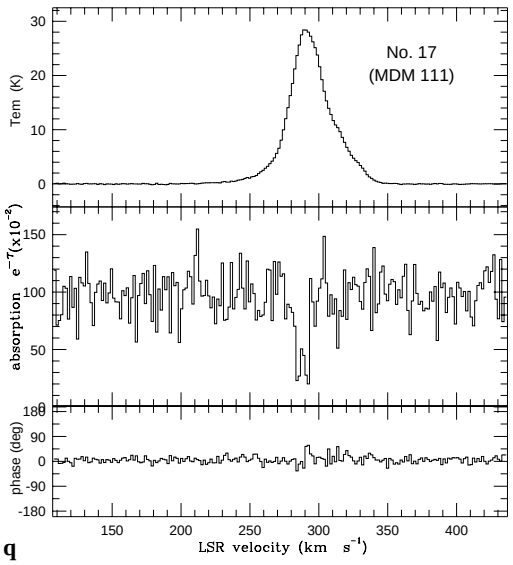

q

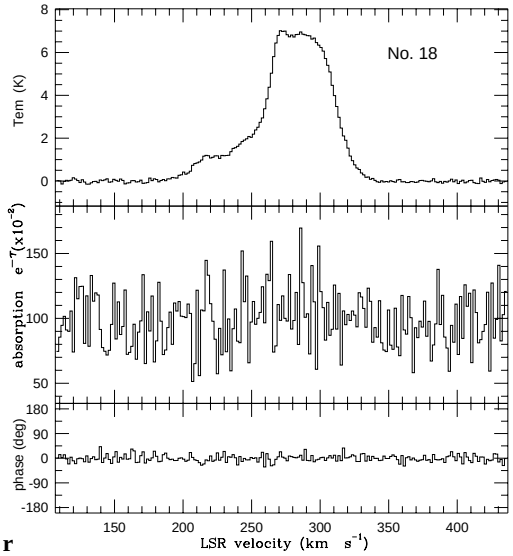

r

Fig. 2a–t. See page 794

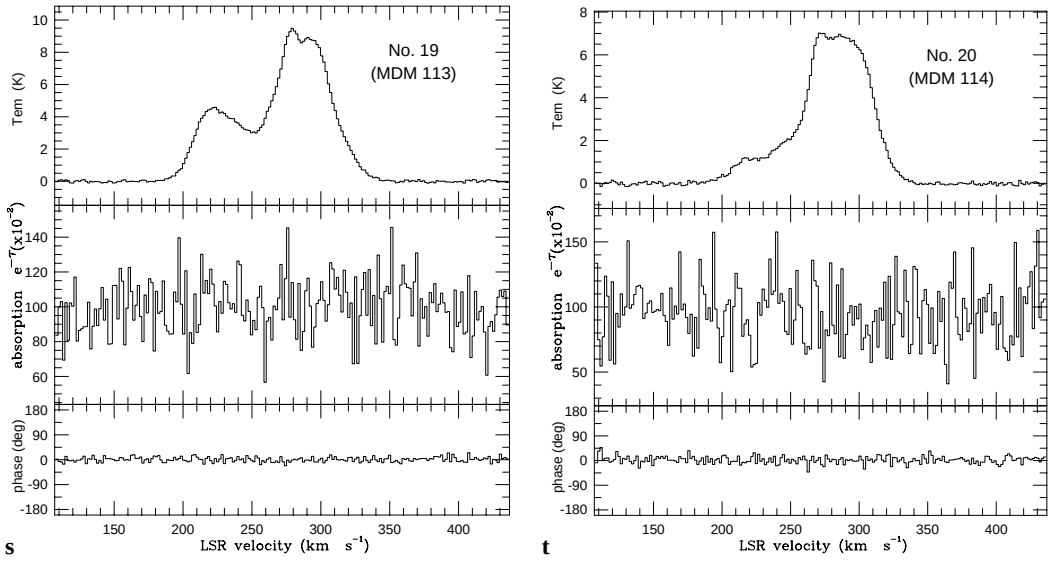

Fig. 2a–t. Emission and absorption spectra toward the continuum sources. The upper panel shows the 21 cm emission spectrum measured with the Parkes telescope (brightness temperature in K) by Luks & Rohlfs (1992), the lower shows the absorption measured with the ATCA (relative absorption $e^{-\tau}$, times 100). At the bottom the interferometer phase as a function of frequency is given in degrees.

sweeping over and around dense H I clouds and so initiating new episodes of star formation (Dopita et al. 1985, Domgörgen et al. 1995). Dopita et al. found an expansion velocity of 36 $\mathrm{km\,s^{-1}}$. As an alternative formation mechanism of LMC 4, a model of HVC-disk collision is discussed by Braun (1996). De Boer et al. (1998) propose that the supergiant structure finds its origin in star formation induced in the bow-shock formed at the leading edge of the LMC. Due to the rotation of the LMC this structure then moved aside.

MDM 31 (No. 4) is to the south of LMC 4, at a projected distance of 1020 pc from the centre position and about 10′ south of the diffuse filament DEM 211. The absorption spectrum shows a deep absorption line ($\tau = 1.64 \pm 0.13$) at 281 $\mathrm{km\,s^{-1}}$. The velocity of this absorption feature is similar to that toward J0526-678 (survey 2), which is 160 pc north-west, but shows higher optical depth. The emission reveals two blended lines, which might be associated with the disk H I and the shell of gas ejected below the plane of the LMC, as analysed by Dopita et al. (1985). The peak of the absorption is offset by about 6 $\mathrm{km\,s^{-1}}$ from the strongest emission peak, the "D" component.

Source **MDM 55 (No. 7)** has a projected distance of 718 pc from the centre of LMC 4. It is located in a region of high column density at the north-eastern rim of DEM231 (N57C), a possible H II region at the ionisation front of the shell. The absorption spectrum shows a narrow and deep absorption line at 279 $\mathrm{km\,s^{-1}}$, the velocity of the disk component. The H I absorption line is similar to that of MDM 31 (No. 4). It shows the same high optical depth.

No absorption has been detected above the detection thresholds toward the other lines of sight in the direction of LMC 4. Source **MDM 25 (No. 3)** is close to the ionized edge of the shell. It is located south of DEM 192 (N51D) in a region of less H I column density compared to MDM 55. There might be a very weak absorption component at 290 $\mathrm{km\,s^{-1}}$, associated with the disk H I but the existence of this cloud has to be verified by further investigations. The sources **MDM 64 (No. 11)** and **MDM 60 (No. 10)** are in the direction of the ionized inner part of the giant shell, near the diffuse Hα region DEM 257. The sources **MDM 44 (No. 6)** and **MDM 58 (No. 9)** are south of DEM 229 (N57) and DEM 245.

The eastern steep H I boundary

Sources **MDM 109 (No. 16), MDM 111 (No. 17), No. 18, MDM 113 (No. 19)** and **MDM 114 (No. 20)** are in the direction of the relatively sharp boundary of the H I gas toward the east of the LMC. Fig. 3 shows the location of the sources on the contour map of the H I column density distribution. A compression zone is hypothesised in this direction of the LMC due to the ram-pressure produced by the motion of the LMC through the gas of the outer galactic halo (Mathewson & Ford 1984).

A detailed search for cool gas in direction of this H I boundary reveals H I absorption toward only one of our sources. Source **MDM 111 (No. 17)** is about 29′ south of J0552-682 (showing H I absorption in survey 2) and about 23′ south of the weak arc-like structure DEM 328. The spectrum shows two deep absorption lines at the velocity of the "D" component. The optical depth of the two lines is a factor of three higher than that toward J0552-682. Both lines of sight are near the cone-like structure at the leading edge, which is seen in the far infrared, and has been discussed by Braun (1996) as likely to be the result of a high velocity cloud impact.

Others

Source **MDM 95 (No. 15)** is about 14′ (200 pc) from source No. 14. It has a projected distance of 600 pc from 30 Doradus. The spectrum shows a small, deep absorption line at 296 $\mathrm{km\,s^{-1}}$, which is offset from the emission peak by about +15 $\mathrm{km\,s^{-1}}$, and two weak absorption lines at about 4 σ_τ. The weak line at 274 $\mathrm{km\,s^{-1}}$ covers a velocity range from 270 to 280 $\mathrm{km\,s^{-1}}$. An absorption feature of similar velocity is seen toward MDM 89 (No. 14). There might be some confusion from emission fluctuations at about 300 $\mathrm{km\,s^{-1}}$. The complex dynamic structure of the cool neutral ISM observed in the vicinity of the Tarantula nebula seems to dissolve near source No. 15. Although the line of sight is only about 160 pc more distant from 30 Doradus than No. 14, the fraction of cool H I compared to the warm (see Sect. 4.1) is a factor of 3 lower.

Source **MDM 20 (Nr. 2)** is about 6.6′ south-east of the diffuse object DEM157 (N128). The very noisy spectrum toward the weak continuum source (26 mJy) shows two tentative absorption lines at 240 $\mathrm{km\,s^{-1}}$ and 264 $\mathrm{km\,s^{-1}}$.

Source **MDM 1 (No. 1)** is about one degree south of the bar. It is in a region of little optical emission, 20.7′ away from DEM102, a small diffuse object. MDM 1 shows a tentative detection of absorption (4 σ_τ) at a velocity of 230 $\mathrm{km\,s^{-1}}$.

Source **MDM 88 (No. 13)** is about 16′ from the diffuse, arc-like structure DEM276 (N214D) and in the direction of the eastern rim of the giant molecular cloud. The absorption spectrum is very noisy in the velocity range of the emission. We are not confident about the weak lines at 264 and 288 $\mathrm{km\,s^{-1}}$ near the detection threshold, which are confined to only one channel.

Source **MDM 32 (No. 5)**, near to the rim of the filamentary and diffuse shell DEM208 (N204) does not show absorption above the detection threshold.

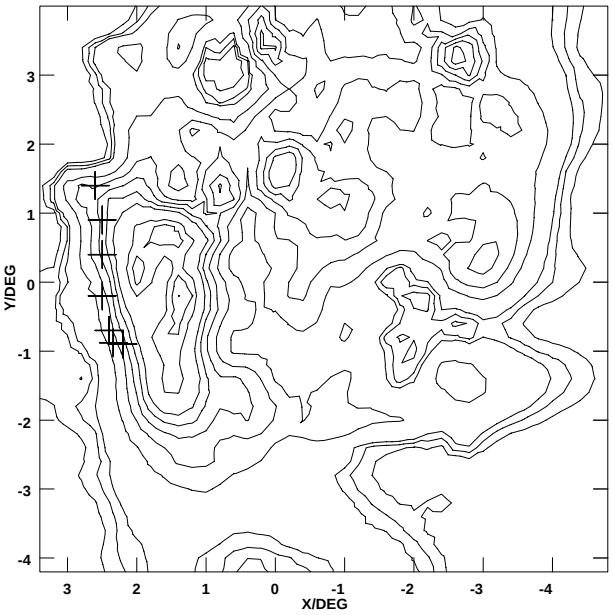

Fig. 3. The positions of sources (survey 2 & 3) at the leading edge of the LMC are superposed on the contour map of the total H I column density (Luks & Rohlfs 1992) at the levels $N_{\rm HI}$ = (2, 3, 4, 7, 10, 14, 18, 22, 29 and 32)×10^{20} $\mathrm{cm^{-2}}$

4. Discussion

4.1. Spectrum integrals: the cool gas fraction

To study the mixture of the warm and cool phases of the interstellar medium along the lines of sight, we have to calculate the velocity integrals of the H I emission and absorption spectra. Results are shown in Table 2. Column 1 gives the source number. The H I column density of the emission and the "equivalent width" of the absorption profile at each line of sight for the entire velocity range (108 to 438 $\mathrm{km\,s^{-1}}$) are given in Columns 2 and 3. $N_{\rm em}$ is computed from the velocity integral of the brightness temperature, $T_{\rm em}$ (v), assuming optically thin emission:

$$\frac{N_{\rm em}}{10^{20}\,\mathrm{cm^{-2}}} = 0.0182 \cdot \frac{\int T_{\rm em}\,(v)dv}{\mathrm{K\,km\,s^{-1}}} \qquad (1)$$

The equivalent width of the absorption profile is defined as the velocity integral

$$EW = \int (1 - \mathrm{e}^{-\tau(v)})dv \qquad (2)$$

The error is calculated from $\Delta EW = \sigma_\tau \cdot \delta v \cdot \sqrt{n}$, where σ_τ is the noise in the optical depth (Table 1, Column 7), δv is the velocity resolution (1.65 $\mathrm{km\,s^{-1}}$) and n=200 is the number of channels included in the integral. In Columns 4 and 5 the column density of the warm gas and the equivalent width of the cool gas are recomputed by integrating only over velocities with $T_{\rm em}$ (v) $>$ 2 K ($N_{\rm em,2K}$, $EW_{\rm 2K}$). This is to separate the contribution to the column density by the warm halo from that by the atomic gas in the LMC proper as discussed in Dickey et al. (1994). As typically fewer than 10 or 15 channels contribute to this sum, the noise in the value of EW is about $\sigma_\tau \cdot \delta v \cdot 4$. Column 6 gives for each line of sight the sum of the equivalent widths of the individual absorption lines (see Table 4, Column 2) for which the optical depth is above the threshold of 3 σ_τ (these values are sketched in Fig. 1). The values of the equivalent width in Columns 3 and 5 also include the contribution from broad, weak absorption components which are below the detection threshold in individual channels, but detectable if the spectrum is heavily smoothed. These marginally-detected contributions make up the bulk of the absorption in our sample, since the background sources are so weak that typically only features with $\tau \geq 0.5$ are securely detected. This is in contrast to most surveys of HI absorption in the Milky Way interstellar medium, which generally use much stronger background sources, allowing detection of lines as faint as $\tau \simeq 0.05$ to 0.1. It is premature to consider the abundance of lines vs. optical depth in the Magellanic Clouds, but our results do not indicate significant differences from the Milky Way result (Garwood & Dickey 1989, Fig. 4).

From the values of EW and $N_{\rm em}$ we can compute the average cool gas fraction by

$$f_{\rm c} \equiv \frac{N_{\rm c}}{N_{\rm c} + N_{\rm w}} = 0.0182 \cdot T_{\rm c} \cdot \frac{(\frac{EW}{\mathrm{km\,s^{-1}}})}{(\frac{N_{\rm em}}{10^{20}\mathrm{cm^{-2}}})} \qquad (3)$$

Table 2. Spectrum integrals

			$T_{\rm em}$>2K				
Source No.	$N_{\rm em}$	EW	$N_{\rm em,2K}$	$EW_{\rm 2K}$	ΣEW_i	$f_{\rm c}$($T_{\rm c}$=60 K)	$f_{\rm c}$($T_{\rm c}$=27 K)
	[$\frac{10^{20}}{\rm cm^2}$]	[$\frac{\rm km}{\rm s}$]	[$\frac{10^{20}}{\rm cm^2}$]	[$\frac{\rm km}{\rm s}$]	[$\frac{\rm km}{\rm s}$]		
(1)	(2)	(3)	(4)	(5)	(6)	(7)	(8)
1	8.5	3.9±2.9	7.6	2.7±1.3	0.7	0.10	0.05
2	14.9	23.7±5.5	14.2	8.9±2.7	3.7	0.28	0.13
3	12.0	4.4±3.4	11.4	-1.4±1.5		< 0.43	< 0.19
4	10.9	9.5±3.0	10.1	3.3±1.3	2.4	0.26	0.12
5	6.2	1.7±3.5	5.4	1.8±1.5		< 0.91	< 0.41
6	14.8	13.8±4.3	13.9	5.7±1.7		< 0.40	< 0.18
7	14.2	4.8±3.6	13.5	2.2±1.4	2.2	0.18	0.08
8	14.5	15.9±3.7	13.9	11.9±1.9	13.1	1.03	0.46
9	11.9	8.4±5.8	11.0	1.0±2.4		< 0.71	< 0.32
10	7.8	4.0±3.8	7.0	1.0±1.6		< 0.75	< 0.34
11	5.6	6.7±2.5	4.4	2.9±1.0		< 0.74	< 0.33
12	32.4	16.3±2.8	31.7	11.4±1.4	9	0.31	0.14
13	29.7	20.3±4.7	29.3	12.5±2.8		< 0.31	< 0.14
14	25.5	7.3±2.3	25.0	7.5±1.2	6.7	0.29	0.13
15	25.5	5.7±2.8	25.0	4.2±1.5	2.2	0.10	0.04
16	11.5	4.8±3.9	11.0	0.4±2.3		< 0.68	< 0.31
17	18.7	12.7±4.3	18.0	8.9±2.1	5.9	0.36	0.16
18	8.0	3.8±4.7	6.7	-4.5±2.2		< 1.07	< 0.48
19	11.7	1.5±3.6	11.2	-2.4±2.2		< 0.64	< 0.29
20	8.0	15.8±5.2	6.7	7.8±2.4		< 1.17	< 0.53

If no absorption is detected we multiply by the upper limit for EW, which is taken to be 3 $\cdot\Delta EW$ (Column 5). $N_{\rm c}$ and $N_{\rm w}$ are the column densities of cool and warm gas. $T_{\rm c}$ is the assumed cloud temperature. Because of the uncertainties in the spin temperature of individual cool clouds, derived in Sect. 4.2, we calculate the fraction of cool gas in the LMC for two mean cloud temperatures, a value of 27 K, implied by the LMC studies (see Sect. 4.2) and a mean cloud temperature of 60 K as found for the Milky Way (Kalberla et al. 1985). The lower value has been confirmed by the study of cloud temperatures in the vicinity of 30 Doradus by Mebold et al. (1997) using high resolution emission- and absorption spectra obtained by combining ATCA and Parkes data. Mebold et al. find values of 30 K to 40 K for the cool diffuse clouds, but we cannot infer from this analysis that all of our cool atomic gas clouds show such low temperatures. The values for $f_{\rm c}$ assuming $T_{\rm c}$= 60 K, the typical value for cool gas clouds in the Milky Way, are given in Table 2, Column 7, the values for $T_{\rm c}$= 27 K are given in Column 8. Fig. 4 a) shows the fraction of cool gas over the face of the LMC for surveys 2&3 using the values of Column 7. Fig. 4 b) and c) present the distribution of the total absorption and the fraction of cool H I with distance from the gravitational centre (Luks & Rohlfs 1992). The angles from the gravitational centre are measured in the rectangular coordinate grid defined by Isserstedt (1975), i.e. $\Theta = \sqrt{(X+1.00^\circ)^2+(Y-0.70^\circ)^2}$ (for the projected distance from the gravitational centre we assume a distance to the LMC of 50 kpc). The lines of sight toward different regions (LMC 4, 30 Doradus complex, eastern H I boundary and the reference group) are distinguished with different symbols.

Obviously, there is no clear decrease in $f_{\rm c}$ with distance from the gravitational centre. A decreasing value of $f_{\rm c}$ could e.g. indicate a pressure gradient gravitationally determined. The fraction of cool gas seems to be rather determined locally by the characteristics of the surrounding objects (e.g. H II regions, SNRs). Cloud formation is most efficient in the star-forming region 30 Doradus and in the direction of LMC 4.

All lines of sight near 30 Doradus show unusually high absorption integrals and a high fraction of cool gas compared to warm. The compact H II region, source No. 8, which is located in the 30 Doradus complex, shows the highest value, $f_{\rm c}$= 1, in the present survey. The high amount of cool gas toward the giant star-forming region, 30 Doradus, is consistent with H I emission/absorption studies toward galactic H II regions (Kuchar & Bania 1989), which show that cool atomic gas is very abundent toward star forming regions. Probably the ISM pressure generated by shock fronts is highest toward the 30 Doradus complex. While the heating rate is only proportional to the number density $\Gamma \propto n$, the cooling rate is given by $\Lambda = \mathcal{L}n^2$, where $\mathcal{L}$ denotes the interstellar cooling function. Local enhanced pressures might increase the density of the gas and force a higher cooling rate.

The high number of cool H I clouds and the high fraction of cool gas compared to warm toward LMC 4 (note that $f_{\rm c}$>60% in the direction of J0526-658 and J0526-678 [survey 2]), also suggest a high cooling rate of gas caused by a high density near the supernova driven shock of LMC 4. The inhomogenity of the distribution of warm and cool gas near LMC 4 suggests a strong clumpiness of the ISM into which the shock wave of LMC 4 propagates.

Cool H I clouds are **not** frequently detected near the eastern steep H I boundary. Cool gas has only been observed in two directions toward the leading edge, which show high column densities and which are near the region, discussed as a possible impact with a High Velocity Cloud by Braun (1996). The fraction of cool H I in these directions is similar to that of empty fields. In contrast to these two directions with detected absorption, the other lines of sight toward the east show a separation of the H I emission into several lines of lower brightness, indicating lower densities and therefore a lower cooling rate.

Table 3 presents a comparison of the fraction of cool gas for the different regions of the LMC as well as the results of averaging over the entire sample of LMC spectra. We add the spectrum integrals, $N_{\rm em}$ and EW, using the values of survey 2 & 3 with the brightness temperature threshold of 2 K (see Table 2, Columns 4 and 5 for survey 3), and thus get totals for the entire sample, $\Sigma_{\rm N}\, N_{\rm em}$ and $\Sigma_{\rm N} EW$ (Table 3, Columns 3 and 4). We find $f_{\rm c}$= 35% if intrinsic continuum sources are included, and $f_{\rm c}$= 32% if they are excluded. In the 30 Doradus complex about half of the neutral hydrogen seems to be in the cool phase. Toward LMC 4 we find 40 per cent cool gas versus 60 per cent warm. This same approach has been used to interpret H I absorption results for disks of other galaxies (Dickey & Brinks 1993), including the Milky Way. Results for high galactic latitude clouds are shown on the bottom of Table 3. From this comparison we find that assuming $T_{\rm c}$= 60 K the interstellar H I of the LMC contains a larger fraction of cool gas than the Milky Way (solar neighborhood). Excluding the nine lines of sight in the direction of the 30 Doradus complex, we find about the same fraction ($f_{\rm c}$= 27 %) of atomic hydrogen in the cool phase as in the solar neighborhood. The values of $f_{\rm c}$ computed here depend, however, on the assumed cool phase temperature $T_{\rm c}$. The value of 60 K used above is a good estimate of $T_{\rm c}$ in clouds at high latitudes in the solar neighborhood, but it may well be that the cool H I in the LMC is colder. For example, if $T_{\rm c}$ were 40 K, we would find $f_{\rm c}$= 0.24% as in the Milky Way. In the extreme case, if $T_{\rm c}$ were as low as 27 K (i.e. mean $T_{\rm sp}$ for both surveys), then the fraction of cool gas would be less than in the Milky Way; $f_{\rm c}$ would be only 0.16.

The LMC differs from the Milky Way also in the overall absorptivity, $h\,\langle\kappa\rangle$, which is calculated in Column 5 (Table 3) by:

$$h\,\langle\kappa\rangle = \frac{\Sigma_{\rm N} \int 1 - {\rm e}^{-\tau} dv}{\sec(i) \cdot (2N_{\rm b} + N_{\rm i})} \qquad (4)$$

where i=33° is the inclination of the disk, $N_{\rm b}$ is the number of background sources and $N_{\rm i}$ is the number of intrinsic sources (for the Milky Way the corresponding value is the equivalent width times sin|b|). Even if we exclude lines of sight near the unusual 30 Doradus region, the LMC shows a higher value for $h\,\langle\kappa\rangle$ than the Milky Way. No other system known shows a value for $h\,\langle\kappa\rangle$ as high as $1\,{\rm km\,s^{-1}}$. Assuming a thickness of the gas disk of the LMC, h, of 300 pc (Kim priv. comm.) we can determine the mean opacity of the H I $\langle\kappa\rangle$ = $6\,{\rm km\,s^{-1}}$ kpc^{-1}. Values for $\langle\kappa\rangle$ in the Milky Way, M31 and M33 are in the range 2 to $5\,{\rm km\,s^{-1}}$ kpc^{-1} (Dickey & Brinks 1993).

4.2. Individual absorption lines: comparison of cloud properties for different regions of the LMC

Nine of the twenty lines of sight show absorption above the 3 σ_τ detection threshold. 20 cool atomic clouds are detected. The cloud properties as derived from the individual absorption features and from the comparison with the H I emission data are shown in Table 4. Column 1 gives the source number, Column 2 the equivalent width of the absorption line. Column 3 shows the peak optical depth, $\tau_{\rm max}$, and Column 4 gives the centre velocity, $v_{\rm cen}$, of the absorption line relative to the LSR. In Column 5 the column density of the emission, $N_{\rm em}$, is listed. We have integrated over just the velocity range of the line component for which the optical depth is above the 3 σ_τ absorption threshold. The absorption line width, σ_v, is given in Column 6. It is calculated by dividing the equivalent width in Column 2 by $\sqrt{2\pi}\tau_{\rm max}$. The upper limits of σ_v of $0.6\,{\rm km\,s^{-1}}$ are determined by the velocity resolution of $1.6\,{\rm km\,s^{-1}}$. Column 7 shows the velocity difference, Δv, between $v_{\rm cen}$ and $v_{\rm disk}$, the velocity of the disk component "D" in direction of the background source: $\Delta v = v_{\rm cen} - v_{\rm disk}$. Values for $v_{\rm disk}$ are from the PhD thesis of Luks (1991) and are listed in Column 8. In some cases the absorption component can be identified with the secondary gas system at lower velocity, the "L" component. We used this term in analogy to Dickey et al. (1994) for all absorption components with $\Delta v < -10\,{\rm km\,s^{-1}}$, even if the emission spectra do not show the "L" component (marked with "L" in Column 9). Lines which are tentative detections near the noise threshold are marked with "?", their velocities are ill-determined. The distribution of the velocity difference Δv is shown in Fig. 5 for all 62 absorption components detected in surveys 2 & 3. The different populations ("L" and "D" component) are shown by different shading. The distribution shows a nearly symmetric shape with a mean velocity of $\langle\Delta v\rangle$ = -0.3 $\pm$ $1.6\,{\rm km\,s^{-1}}$ and a dispersion in velocity of $\sigma_{\Delta v}$ = $12.4\,{\rm km\,s^{-1}}$. Considering only the 35 lines marked "D", we find a mean value $\langle\Delta v\rangle$ = 3.1 $\pm$ $1.2\,{\rm km\,s^{-1}}$ and a dispersion in velocity of $7.3\,{\rm km\,s^{-1}}$. This value does not significantly differ from the one found by Dickey et al. (1994) and is close to the true random velocity dispersion of the cloud population in the LMC disk.

Column 10 of Table 4 lists the values for the spin temperatures calculated for the individual line components at their centre velocity:

$$T_{\rm sp} = \frac{T_{\rm em}}{1 - e^{-\tau_{\rm max}}} \qquad (5)$$

We find a mean cloud temperature of 29 K in agreement with the value of 25 K derived from survey 2. The calculated spin temperatures are apparent ones, because we assume the H I emission to be distributed homogeneously over the entire 15′ Parkes beam and we do not take into account mixing of gas at different temperatures in each velocity channel. From the present data, we can not isolate discrete emission features at the velocities of the absorption features. Most of the emission observed with Parkes must come from the warm gas. The presence of emission fringes on the shortest baselines of the ATCA (77 m to 800 m) indicates that there is structure in the 21 cm emission on scales of 9′ to

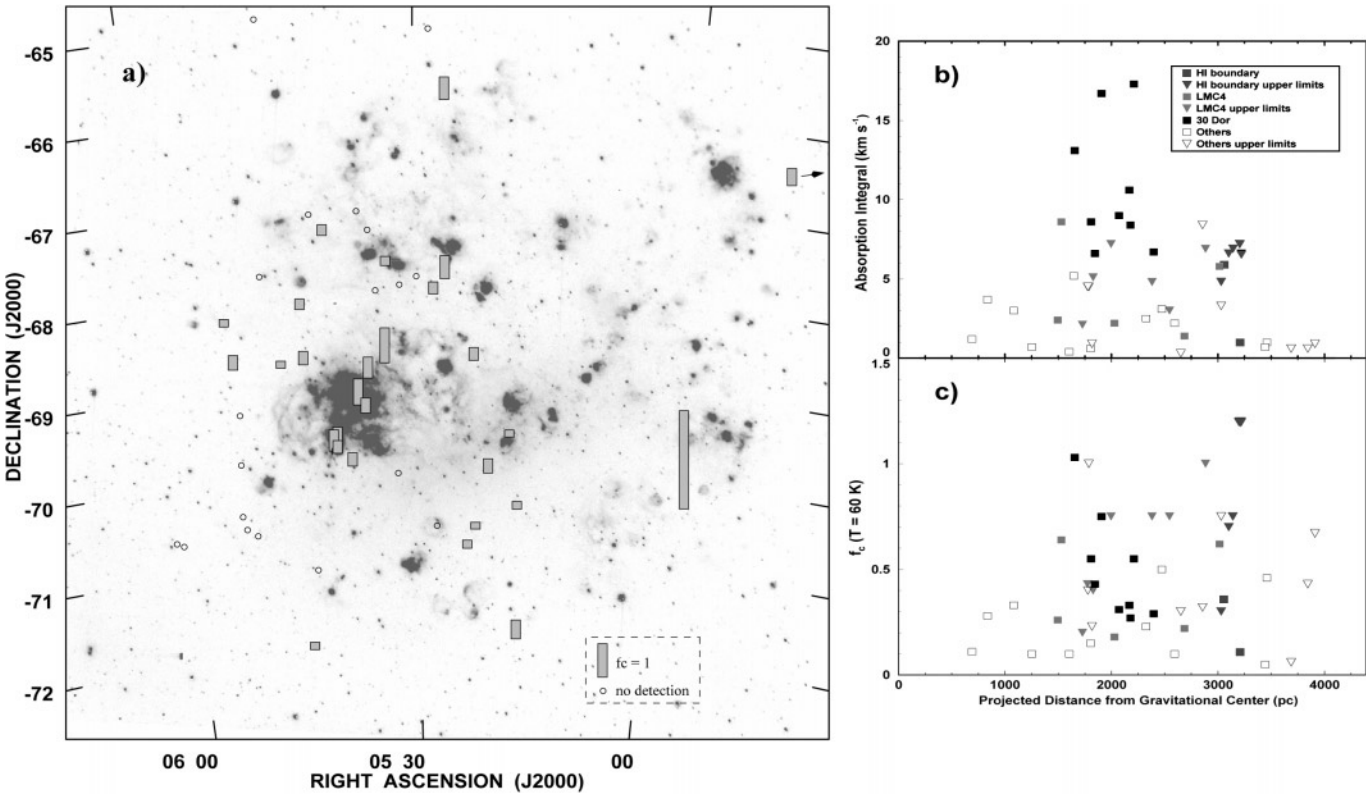

Fig. 4a–c. The fraction of cool gas, $f_c(T_c = 60\,\mathrm{K})$, compared to the warm for H I absorption survey 2&3 is shown on the left over the face of the LMC. The unphysically high value at the west side of the LMC (J0456-702) is due to a very low temperature of the gas in this direction (Paper II). On the right, the absorption integral and the fraction of cool gas is plotted against the projected distance from the gravitational centre, except the value of f_c for J0456-702.

Table 3. Comparison of $h\,\langle\kappa\rangle$ and f_c with the Milky Way

Summing lines of sight ("weighting by mass"):						
N	Sample	$\Sigma_N N_{em}$ $[\frac{10^{20}}{cm^2}]$	$\Sigma_N EW$ $[\frac{km}{s}]$	$h\,\langle\kappa\rangle$ $[\frac{km}{s}]$	$f_c(T_c$=60 K) [%]	$f_c(T_c$=27 K) [%]
(1)	(2)	(3)	(4)	(5)	(6)	(7)
LMC:						
49	All sources[2]	621	201	1.79	35	16
45	Background only	505	150	1.40	32	15
40	Without 30 Dor complex	390	96	1.01	27	12
LMC regions:						
9	30 Dor complex	231	97	5.42	46	21
5	LMC 4	56	20	1.68	39	18
2	East	28	7	1.47	27	12
12	Others	113	24	0.84	23	10
The Milky Way:						
19	$30° > \|b\| > 10°$, Arecibo samples			0.72	24	

[2]The background source J0545-648 (survey 2) is left out because we have no emission information in this area

54″ (≈131 to 13 pc) (K. Rucker 1995). A comparison with the ATCA-H I-Mosaic of the LMC (Kim et al. 1997) also reveals small emission structures for several lines of sight with cool H I gas.

The last column shows the values of the "Doppler temperature", i.e. the equivalent temperature for which the line width would result from thermal broadening alone

$$T_{\mathrm{Dopp}} = \frac{\mathrm{m}\cdot\sigma_v^2}{\mathrm{k}} = 121\cdot(\frac{\sigma_v}{\mathrm{km\,s^{-1}}})^2\,[\mathrm{K}], \quad (6)$$

Table 4. Individual absorption lines

Source No.	EW [$\frac{\mathrm{km}}{\mathrm{s}}$]	$\tau_{\max}$	v_{cen} [$\frac{\mathrm{km}}{\mathrm{s}}$]	N_{em} [$\frac{10^{20}}{\mathrm{cm}^2}$]	σ_v [$\frac{\mathrm{km}}{\mathrm{s}}$]	Δv [$\frac{\mathrm{km}}{\mathrm{s}}$]	v_{disk} [$\frac{\mathrm{km}}{\mathrm{s}}$]	System	T_{sp} [K]	T_{Dopp} [K]
(1)	(2)	(3)	(4)	(5)	(6)	(7)	(8)	(9)	(10)	(11)
1	0.7±0.2	0.54	230	0.2	<0.6	−11	241	?	15	weak
2	2.5±0.5	1.47	240	0.6	0.7	−30	270	?	8	weak
	1.2±0.4	1.23	264	0.4	<0.6	−6		?	11	weak
4	2.4±0.3	1.64	281	1.1	<0.6	+6	275	D	11	<43
7	2.2±0.4	1.64	279	1.8	<0.6	−4	283	D	20	<43
8	13.1±0.9	1.64	248	5.2	3.2	−23	271	L_i	10	blend
12	1.4±0.3	0.59	238	2.3	0.9	−11	249	L	69	98
	5.3±0.4	1.59	243	7.2	1.3	−6		D	30	204
	0.9±0.2	0.81	253	1.3	<0.6	+4		D	54	<43
	0.7±0.2	0.52	261	0.8	<0.6	+12		D	51	<43
	0.7±0.2	0.55	264	0.6	<0.6	+15		D	35	<43
14	2.6±0.3	0.87	258	2.1	1.2	−12	270	L	24	174
	2.6±0.3	1.40	264	2.5	0.7	−6		D	19	59
	0.8±0.2	0.66	271	0.9	<0.6	+1		D	45	<43
	0.7±0.2	0.56	276	0.9	<0.6	+6		D	51	<43
15	0.6±0.2	0.48	274	0.7	<0.6	−7	281	D	51	<43
	1.0±0.2	0.94	296	0.6	<0.6	+15		D	22	<43
	0.6±0.2	0.47	306	0.3	<0.6	+25		?	25	weak
17	2.5±0.4	1.47	284	1.5	0.7	−7	291	D	16	59
	3.4±0.5	1.61	293	2.5	0.8	+2		D	17	77

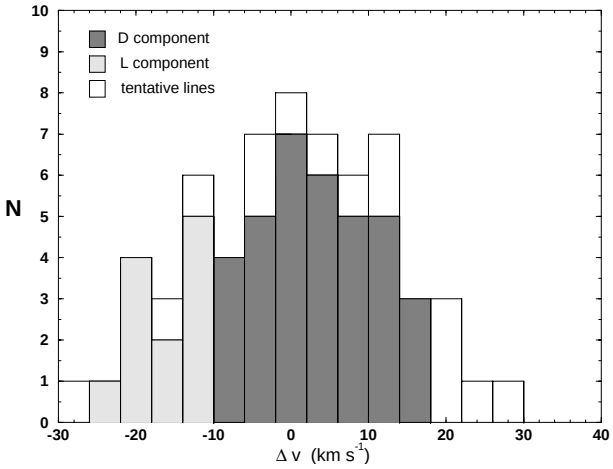

Fig. 5. For the absorption surveys 2 & 3 the distribution of the deviations (Δv) of velocities of absorption components from the disk velocity is shown. The shading distinguishes between the low velocity component "L", the disk component "D" and tentative lines "?". The velocity dispersion of the entire set of lines is 12.4 $\mathrm{km\,s^{-1}}$, for the "D" population alone it is 7.3 $\mathrm{km\,s^{-1}}$.

where m is the hydrogen mass and k is Boltzmann's constant. T_{Dopp} is a weak upper limit on the kinetic temperature of the gas seen in absorption (see Dickey et al. 1994). The limit of 43 K for the "Doppler temperatures" is the result of the velocity resolution.

The difference in cloud parameters among the 30 Doradus complex, LMC 4, the eastern H I boundary and the reference sample are illustrated in Fig. 6. The values of the equivalent width (Fig. 6a), the optical depth (Fig. 6b) and the spin temperatures (Fig. 6c) from surveys 2&3 are plotted against the projected distance from the gravitational centre. Lines of sight toward different regions are distinguished with different symbols. Mean values per distance interval of 250 $\mathrm{km\,s^{-1}}$ are shown by dotted lines, mean values of the four different groups are plotted on the right margin. We do not find a dependence of the mean values of τ or EW on the distance from the gravitational centre. The mean temperature (dotted line in Fig. 6 c) increases over the face of the LMC, which is consistent with the non-detection of cool gas in the halo of the LMC. Atomic clouds toward the 30 Doradus complex show the highest values of EW, τ and T_{sp}, but also a striking scatter of all cloud parameters. Unusually high values of EW, above 13 $\mathrm{km\,s^{-1}}$ are detected toward J0540-697 (survey 2) and source No. 8. Both sources are associated with regions of recent star formation. The high value of EW seems to be due to a high number of unresolved clouds with similar velocities. Clouds in the direction of LMC 4 and the leading edge of the LMC also differ from atomic clouds at the reference positions by higher values of EW and τ. Their mean optical depths are not significantly different from that of the 30 Doradus complex. About half of the cool clouds near 30 Doradus, near LMC 4 and near the eastern steep H I boundary are optically thick, whereas most clouds in other regions show low values of τ. This implies higher densities of the cool atomic gas toward 30 Doradus, LMC 4 and the eastern H I boundary compared to other regions of the LMC.

Comparing the cloud properties with those of galactic cool H I clouds (Dickey et al. 1978), we find that LMC clouds show higher values of EW and τ. For all lines of sight the mean

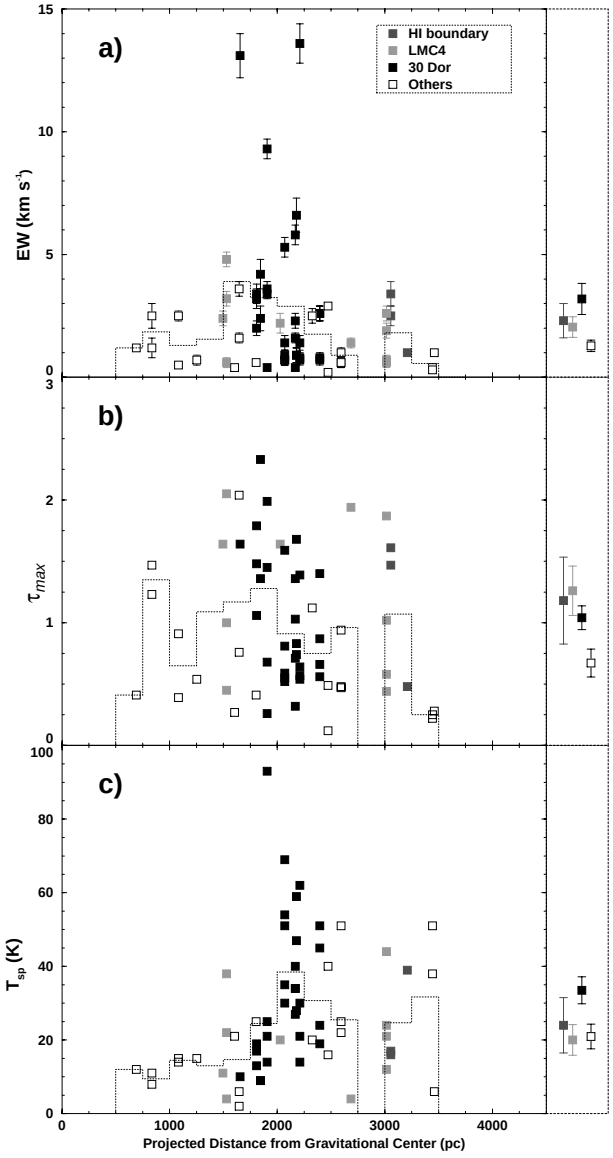

Fig. 6a–c. Equivalent widths, optical depth and spin temperature of detected absorption lines on the individual lines of sight versus the projected distance from the gravitational centre. Values for lines of sight near 30 Doradus, near LMC 4 and toward the eastern steep H I boundary are marked with different symbols. The dotted line shows mean values of EW per distance of 250 pc. The mean values for the four different groups are plotted on the right margin.

value of $\langle EW \rangle$ is 2.39 $\mathrm{km\,s^{-1}}$, which is a factor of six higher than the mean value from high galactic latitude clouds ($|b| > 25°$), $\langle EW \rangle$ = 0.38 $\mathrm{km\,s^{-1}}$. Even the reference group has a higher value of $\langle EW \rangle$= 1.23 $\mathrm{km\,s^{-1}}$, which is similar to that of intermediate galactic latitude clouds ($|b| < 20°$), $\langle EW \rangle$ = 1.28 $\mathrm{km\,s^{-1}}$. The mean value of the optical depth, $\langle \tau \rangle$= 1.01, is a factor of 6 higher than the value found for high latitude clouds in the Milky Way, $\langle \tau \rangle$= 0.18, but is similar to that found for the inner Milky Way, $\langle \tau \rangle$= 0.83 (Garwood & Dickey 1989). Clouds toward LMC 4, 30 Doradus and the leading edge show mean values of τ above 1, the reference sample shows a value of 0.67.

5. Conclusions

We have used the ATCA to measure H I absorption toward 20 continuum sources in and behind the LMC. The lines of sight are mainly in directions of the 30 Doradus complex, toward the supergiant shell LMC 4 and toward the eastern steep H I boundary. We have identified 20 absorption features toward nine of the 20 sources with a 3 σ_τ detection threshold between 0.33 and 0.75. The derived spin temperatures for the cool atomic clouds range from 8 K to 69 K. The cool gas parameters i.e. the optical depth τ, the "equivalent width" EW, the spin temperature $T_{\rm sp}$ and the cool gas fraction $f_{\rm c}$, have been compared for the different regions of the LMC taking the results of the previous H I absorption survey of Dickey et al. (1994, survey 2) into account.

The cool gas clouds toward 30 Doradus and LMC 4 differ from clouds far from star forming regions and shock fronts in having higher values of EW and τ and in a higher fraction of cool gas. The 30 Doradus complex shows an unusually large amount of cool H I about half of the atomic neutral hydrogen. We know of no other galaxy which possesses regions with that high fraction of cool H I gas compared to the warm. The cool gas in the vicinity of 30 Doradus shows a complex dynamic structure even beyond the optical part of this giant star forming region. Whereas all lines of sight toward the 30 Doradus complex show cool H I clouds, only about half of the lines of sight toward LMC 4 reveal H I absorption features. Cool H I clouds have been even less frequently detected in the direction of the eastern steep H I boundary. The number of detected cool H I clouds and their properties suggests a higher cooling rate near LMC 4 and 30 Doradus compared to the reference positions, caused by an enhanced density near shock fronts. We do not find a statistically significant enhancement of cool clouds toward the eastern boundary of the LMC, in spite of an expected compression zone due to the motion of the galaxy through the halo of the Milky Way. But the detected cool H I clouds at the leading edge differ from atomic clouds at reference positions by higher values of EW and τ, which seems to indicate a higher cooling rate of gas behind a large shock on the east side. The distribution of cool H I suggests a higher compression of gas on the north end of this boundary.

From the present H I absorption studies we conclude that the fraction of cool gas in the LMC is determined by local conditions of the ISM (e.g. H II regions, SNRs), rather than by the distance from the gravitational centre.

The new data corroborate the earlier suggestion that the H I clouds in the LMC are either unusually cool ($\langle T_{\rm c} \rangle \approx 30$ K) compared to the cool phase in the Milky Way ($\langle T_{\rm c} \rangle$ = 60 K), or that the cool atomic phase of the interstellar medium is more abundant in the LMC ($f_{\rm c}$= 35% for $T_{\rm c}$ = 60 K) relative to the warm neutral medium than in our Galaxy ($f_{\rm c}$= 24% for $T_{\rm c}$ = 60 K). Even, if we exclude lines of sight toward the 30 Doradus complex and toward LMC 4 we find, assuming $T_{\rm c}$ = 60 K, a similar mixture of warm and cool interstellar phases compared to that in the Milky Way, despite the completely different radiation field, heavy element abundance and dust-to-gas ratio among these galaxies.

Acknowledgements. We would like to thank S. Ames and K. de Boer for helpful comments on the manuscript. Part of this project was supported by *Deutsches Zentrum für Luft- und Raumfahrt e.V., DLR*, project number 50OR9615 and *Cusanuswerk*, Bonn.

References

Blondiau M.J., Kerp J., Mebold U., Klein U., 1997, A&A 323, 585
Braun M., 1996, Astron. Nachr. 317, 369
Caulet A., Deharveng L., Georgelin Y.M., Georgelin Y.P., 1982, A&A 110, 185
Cohen R.S., Dame M.T., Garay G., et al., 1988, ApJ 331, L95
de Boer K.S., Braun J.M., Vallenari A., Mebold U., 1998, A&A 329, 49
Dickey J.M., Salpeter E.E., Terzian Y., 1978, ApJS 36, 77
Dickey J.M., Brinks E., 1993, ApJ 405, 153
Dickey J.M., Mebold U., Marx M., et al., 1994, A&A 289, 357
Domgörgen H., Bomans D.J., de Boer, 1995, A&A 296, 523
Dopita M.A., Mathewson D.S., Ford V.L., 1985, ApJ 297, 599
Garwood R.W., Dickey J.M., 1989, ApJ 338, 841
Isserstedt J., 1975, A&A 41, 21
Kalberla P.M.W., Schwarz U.J., Goss W.M., 1985, A&A 144, 27
Kennicutt R.C., Bresolin Jr., Bresolin F., et al., 1995, AJ 109, 594
Kim S., Staveley-Smith L., Sault R.J., et al., 1997, PASA 14, 119
Kuchar T.A., Bania T.M., 1989, ApJ 352, 192
Luks Th., 1991, Ph.D. Thesis, Ruhr-Universität Bochum, Strukturanalyse des interstellaren Mediums der Großen Magellanschen Wolke nach Linienprofilen des neutralen Wasserstoffs
Luks Th., Rohlfs K., 1992, A&A 263, 41
Marx M., Dickey J., Mebold U., 1997, A&AS 126, 325
Mathewson D.S., Ford V.L., 1984, IAU Symp. 108, 125
Meaburn J., 1980, MNRAS 192, 365
Mebold U., Greisen E.W., Wilson W., et al., 1991, A&A 251, L1
Mebold U., Düsterberg C., Dickey J.M., Staveley-Smith, L., Kalberla P., 1997, ApJ 490, L65
Mochizuki K., Nakagawa T., Doi Y., et al., 1994, ApJ 430, L37
Radhakrishnan V., Murray J.D., Lockhart P., Whittle R.P.J., 1972, ApJS 24, 15
Rucker K., 1995, Diploma Thesis, Radioastronomisches Institut der Universität Bonn, Emissionsfluktuationen der 21cm Linienemission in der LMC
Stanimirovic S., Staveley-Smith L., Dickey J.M., Sault R.J., Snowden S.L., 1999, MNRAS 302, 417
Thompson A.R., Moran J.M., Swenson G.W. Jr., 1986, Interferometry and Synthesis in Radio Astronomy. John Wiley and Sons, New York, p. 160
Wolfire M.G., Hollenbach D., McKee Ch.F., Tielens A.G.G.M., Bakes E.L.O., 1995, ApJ 443, 152